CMOS Solid-State Photomultiplier for Detecting Scintillation Light in Harsh Environments

C.J. Stapels, W.G. Lawrence, and J.F. Christian[1]
Radiation Monitoring Devices, Inc., Watertown, MA 02472, USA

F.L. Augustine
Augustine Engineering, Encinitas, CA 92024, USA

A CMOS SSPM coupled to a scintillation crystal uses an array of CMOS Geiger-mode avalanche photodiode (GPD) pixels to collect light and produce a signal proportional to the energy of the radiation. Each pixel acts as a binary photon detector, but the summed output is an analog representation of the total photon intensity. We have fabricated arrays of GPD pixels in a CMOS environment, which makes possible the production of miniaturized arrays integrated with the detector electronics in a small silicon chip. In this work, we compare designs for the CMOS GPD pixel used in the SSPM detector and present preliminary results in constructing a solid-state photomultiplier. One pixel design achieves maximum detection efficiency for 632-nm photons approaching 30% with a room temperature dark count rate of less then 1 kHz for a 30-μm-diameter pixel. We characterize the after pulsing in a CMOS GPD pixel, and the crosstalk between CMOS GPD pixels. We examine SSPM design considerations and the effects of after pulsing and cross talk on the performance of the SSPM detector.

1. INTRODUCTION

Nuclear and high-energy physics experiments often require photo-detectors to measure light from scintillation detectors in harsh environments, such as milliKelvin temperatures of a helium dilution refrigerator, and strong magnetic fields. Such conditions limit the utility of many conventional photo-detection technologies. An array of avalanche photodiode pixels operated in Geiger mode, referred to as a solid-state photomultiplier (SSPM), provides an alternative, robust platform for detecting scintillation photons in harsh environments.

Although scintillating materials are ideal for detecting and measuring high-energy radiation, the limitations of existing optical detectors reduces their functionality by necessitating the addition of ancillary circuit components. Replacing the photomultiplier tube (PMT), and its supporting electronics, with an appropriate CMOS technology would provide a fully integrated, low-cost solution to optimize the functionality of scintillation materials, which is essential for applications such as the development of deployable digital dosimeters.

1.1. SSPM Operating Principle

An SSPM is an array of avalanche photodiodes operating in Geiger mode, referred to as Geiger photodiodes (GPDs). The SSPM achieves the low noise of a PMT at a low cost while retaining the high quantum efficiency of a silicon device. The SSPM provides a basis for radiation spectrometers with a wide range of applications. Since the light produced in the scintillation material is proportional to the energy of the absorbed event, the number of pixels that fire provides the energy of the incident photon when the SSPM is uniformly illuminated. Figure 1 illustrates the principle of operation of the SSPM.

P. Buzhan *et al.* have shown that this method approaches and exceeds the performance of a standard
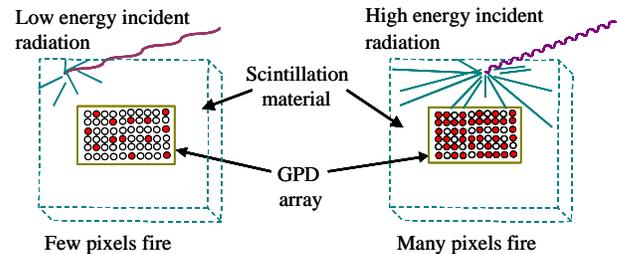
Figure 1: SSPM principal of operation. Nuclear and high-energy photons strike the scintillation crystal and produce visible light proportional to their energy. The number of pixels that fire in the GPD array is thus a function of the energy of the incident event.

PMT for detection of the optical photons from a scintillation detector in certain applications [1]. Implementing this approach in a CMOS-compatible process will allow high precision, low-cost sensors with the additional benefit of monolithic integration of signal processing electronics.

We have fabricated several CMOS-based test arrays of these pixel sensors and characterized their performance as individual detectors, and as arrays. Figure 2 presents a photograph of a chip with test arrays, where the long rectangular shape maximizes the number of contact pads for test points.

Figure 2: Photograph of CMOS APD chip that contains three nine-element arrays, and eight active quenching circuits. The arrays have 60-, 80- and 150-μm spacing; each array has two independent elements and seven summed elements. Test pixels with various sizes are included on the left.

In the SSPM, the individual pixels are biased above their reverse-bias breakdown voltage, which is referred to as Geiger-mode operation. Various aspects of the performance and operation of GPD pixels, fabricated with custom processes, have been studied [2-8]. The design of the CMOS pixel described in this work, specifically

---

referred to as design 12, is similar to that of Rochas *et al.* [9]. In this work, we estimate the optimum design and expected performance of a CMOS SSPM detector using pixel characteristics.

2. SSPM PERFORMANCE MODELING

We are interested in modeling the anticipated SSPM performance using readily measured characteristics of the CMOS GPD pixels to optimize the design of the SSPM. The following list summarizes these characteristics: the size of the pixel, the size of the array, the fill-factor, the operating bias, the detection efficiency (DE) of the GPD pixel, the DCR of the GPD pixels in the array, the fill factor, the after pulsing gain factor, and the cross talk gain factor. In this work, we examine the following list of SSPM performance characteristics:

1   SSPM DE
2   SSPM intensity range and energy resolution
- Source intensity range & after pulsing
- Energy resolution: & cross talk
3   SSPM sensitivity
- SSPM room temperature dark noise
- Effects of after pulsing and cross talk on SSPM noise

Geiger pulses typically exhibit very good pulse height uniformity, so Geiger pulse height variations have been neglected in the modeling presented in this work.

2.1. SSPM Detection Efficiency

The first important characteristic of an SSPM detector is its detection efficiency. The single optical-photon detection efficiency of the SSMP detector can be measured with a calibrated light source; however, we are interested in determining the anticipated detection efficiency as various design and operating parameters are varied. The single-optical photon SSPM detection efficiency, η_d, depends on the detection efficiency of the individual pixels, and the fill-factor, or active area, of the pixel on the SSPM chip, as expressed in Equation 1:

$$\eta_d(\lambda, V_x) = f(\Delta x, A_r)\, \eta_d(\lambda, V_x)\,, \qquad (1)$$

where f stands for fill factor, which is a function of the pixel spacing, Δx, and the pixel area, A_r. For the detection efficiency and dark count rate, described later, bold face represents a property of the SSPM device, and normal type represents the property of a single pixel. The η_d term represents the detection efficiency of a single pixel, which depends on the wavelength of the photon, λ, and Vx represents the excess bias voltage, as defined by the following equation:

$$V_x = V - V_B\,, \qquad (2)$$

where V is the bias voltage applied to the array, and V_B is the avalanche breakdown voltage of a typical APD pixel. The variation in the breakdown voltage of pixels in an array is typically less than 50 mV.

The detection efficiency (DE) of the pixel depends on the quantum efficiency (QE) and the bias-dependent Geiger probability. The QE, which represents an upper limit for the DE, arises from measurements of the CMOS GPD pixel element when they are operated as unity-gain photodiodes. The DE describes the probability that an incident photon will produce a Geiger event in the pixel, which arises from measurements of the CMOS GPD pixel when operated in Geiger mode, i.e., above its reverse-bias breakdown voltage.

When measuring the pixel detection efficiency, we must correct for the effects of after pulsing on the detection efficiency measurement [10]. The after pulsing essentially inflates the measured detection efficiency, referred to as the apparent detection efficiency, by the gain factor associated with the after pulsing. This effective gain factor is described below.

2.2. SSPM Range and Resolution

When the SSPM detects events from a scintillation crystal, the event rate is proportional to the intensity of the source, and the energy of the event in the crystal is proportional to the number of pixels that fire. The maximum count rate of a single GPD pixel determines the maximum event rate, or range, of the SSPM detector, and the number of pixels in the array determines the energy resolution of the SSPM detector.

Two characteristics that affect the SSPM rand and resolution performance are after pulsing and cross talk. The after pulsing affects the maximum source intensity that can be measured with the SSPM, and the cross talk affects the energy resolution of the SSPM. An effective multiplication factor, M_a and M_x, quantifies both the after pulsing and cross talk, respectively.

2.2.1. SSPM Intensity Range and After Pulsing

In a single GPD pixel, the delayed release of trapped charge produces an after pulse that is correlated to an initiating Geiger event. After pulsing produces time-correlated "bunches" of Geiger pulses from a single pixel after an initial Geiger event. This introduces a "dead time" that limits the maximum event rate, or source intensity, that can be measured without saturation effects. Since all GPD pixels are operated in parallel, the maximum count rate in the SSPM is approximately the same as that of a single GPD pixel, and is described by Equation 3.

$$R_{\max} = \frac{I_{\max}}{\Delta t} = \frac{\gamma\, I_0}{\tau\, M_a}\,, \qquad (3)$$

where $R_{\max}$ represents the maximum event rate, $I_{\max}$ represents the total counts in a measurement time period of Δt, and I_0 is the intensity of the source. The γ factor is the efficiency for detecting the radiation at the location of the scintillation detector, and τ represents the time constant associated with the Geiger pulse; the time constant for a 100-kΩ-actively-quenched, 30-μm-diameter CMOS GPD pixel is ~5 μs. The effective multiplication factor introduced by the after pulsing, M_a, represents the average number of pulses produced by an initiating Geiger event in a single pixel.

As mentioned earlier, the true single-photon detection efficiency of the GPD pixel must be corrected for the additional signal generated by the after pulsing. Equation 4 relates the true GPD detection efficiency to the measured DE with after pulsing contributions.

$$\eta_d(\lambda, V_x) = \left(\frac{\Delta I}{M_a}\right)\left(\frac{A_{\text{cal}}}{A_r}\right)\left(\frac{e\,\eta_{\text{cal}}}{\Delta i}\right), \qquad (4)$$

where ΔI refers to the count rate, light counts minus dark counts in Hz, of the GPD pixel, and A_{cal}, η_{cal} and Δi refer to the area, quantum efficiency and photocurrent of a calibrated photodiode that experiences the same illumination as the GPD pixel. The M_a term corrects for the larger count rates measured in the presence of after pulsing.

2.2.2. SSPM Energy Resolution and Cross Talk

In the SSPM, cross talk between pixels causes the pixels to fire in spatially localized "bunches" when triggered by a single-optical photon from the scintillation material. The emission of light from hot carriers [11-13] in a triggered pixel produces this cross talk. The average number of pixels that fire in a bunch represents an effective gain factor, M_x, which reduces the effective number of pixels in the array, and thus SSPM energy resolution. Equation 5 expresses the anticipated SSPM amplitude resolution, or energy resolution, in the presence of cross talk characterized by the gain factor, M_x:

$$\Delta A = 1 + (N/M_x) \propto \Delta E, \qquad (5)$$

where ΔA specifies the amplitude resolution of the SSPM, N is the total number of pixels in the SSPM and ΔE is the energy resolution of the SSPM. The effective multiplication factor introduced by cross talk, M_x, represents the average number of pixels that fire in an array for a single optical-photon event.

When the dark count rate of the SSPM is negligible, because either the size of the GPD array is small, or the SSPM is cooled, then the cross talk can be measured by triggering a single pixel with a focused laser pulse, and measuring the resulting pulse height distribution. The cross talk gain factor is simply the average of this pulse height distribution. In principle, the cross talk measured by triggering a pixel at the edges of the device should differ from that measured by triggering a pixel in the center of the SSPM, however, using a crystal that under fills the SSPM detector reduces these edge effects.

In this work, we measure the cross talk gain factor between a pair of pixels, m_x, as a function of bias and pixel spacing; we then extrapolate the cross talk gain factor, M_x. Equation 6 defines the pair wise cross talk gain factor.

$$m_x = \frac{I_1 + I_2}{i_1 + i_2}, \qquad (6)$$

where I_1 and I_2 refer to the count rate in pixels 1 and 2, respectively, when both pixels are operating simultaneously. The symbols i_1 and i_2 refer to the count rate of the isolated pixel, which is measured when the other pixel is unbiased. In addition, we assume that a simple phenomenological function, defined in Equation 7, describes the dependence of the cross talk on the excess bias and pixel spacing.

$$\frac{1}{m_x} \cong 1 - \frac{\alpha\,V_x}{r^2}, \qquad (7)$$

where α is a constant recovered from a fit to the data, and r is the distance between the pixels.

To extrapolate the cross talk gain factor, M_x, Equation 8 sums the contributions of the pair wise gain factors from the other pixels in the array.

$$\frac{1}{M_x} \cong 1 - \frac{\alpha\,V_x}{\Delta x^2}\left(4 \times \sum_{k=1}^{\frac{1}{2}\sqrt{N}} \sum_{j=0}^{k} \frac{1}{(k^2 + j^2)}\right), (8)$$

This expression must be bounded by zero, such that, $1/M_x > 0$. This expression sums the pair wise gain of a given pixel element with all other pixels in the square array, and it assumes that the triggered pixel is in the center of the array. The Δx term is the distance between two adjacent pixels, i.e., the pixel pitch, for a given SSPM layout. The following expression describes an approximation for the terms in the parenthesis of Equation 8.

$$4 \times \left[1.6 + 0.79\log\left(\frac{\sqrt{N}}{2} - 0.15\right)\right]. \qquad (9)$$

This approximation provides a function of N without the nested summation terms. Given an estimate of M_x, we can not only estimate the amplitude resolution of the SSPM, but also the noise added to the signal from the cross talk, discussed below.

2.3. SSPM Sensitivity

The SSPM sensitivity refers to the lowest event energy, or smallest scintillation amplitude, that can be detected by the SSPM. The noise floor produced by thermally generated Geiger pulses, or dark counts, for the sum of all pixels in the array limits the sensitivity of the SSPM detector. Fluctuations in the signal caused by cross talk and after pulsing, analogous to gain fluctuations, also affect the sensitivity of the SSPM detector by broadening the thermal noise baseline.

2.3.1. SSPM Room Temperature Dark Noise

In the absence of cross talk and after pulsing, the dark counts will produce an amplitude spectrum, which defines the noise floor. A Poisson distribution, Equation 10, characterizes this idealized noise floor when operating the GPD array as an SSPM at room temperature.

$$P(n) = \frac{(I_d\,\tau)^n}{n!}\exp(-I_d\,\tau), \qquad (10)$$

where $P(n)$ describes the probability for generating an n-photon event from the thermally generated dark counts in the SSPM, and n represents the number of pixels triggered by an event, which is the number of detected photons for the scintillation event. The term I_d denotes the dark count

rate of the SSPM, which is the sum of the dark count rate for each of the individual pixels.

Equation 11 approximates the dark count rate of the SSPM, I_d:

$$I_d \cong N\, I_d \,. \tag{11}$$

In this equation, I_d represents the dark count rate of a "typical" pixel. The I_d (bold face) and I_d terms depend on both the temperature and the excess bias.

2.3.2. After Pulsing and Cross Talk Effects

Figure 3 illustrates the "zeroth order" effects of after pulsing and cross talk on a hypothetical pulse height spectrum from an SSPM detector.
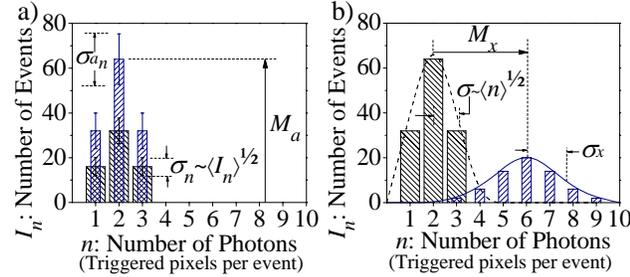
Figure 3: Illustration of the effect of a) after pulsing and b) cross talk on the SSPM signal in a pulse height spectrum. The fat black bars, with left-high to right-low hatch, represents the pulse height spectrum without after pulsing or cross talk. In a), the after pulsing increases the number of events for each n-photon channel by the multiplication factor M_a. The after pulsing also increases the fluctuations, σ_{a_n}, in the number of events in each channel. In b), the cross talk increases the mean amplitude of the pulse height distribution, by the multiplication factor M_x; it also increases the width of the pulse height spectrum, σ_x.

The illustration shows the effect of the gain factors, M_a and M_x, on the pulse height signal, which, as discussed above, affects the maximum source event rate and amplitude resolution of the SSPM detector, respectively. This "zeroth order" illustration assumes that the after pulsing does not affect the shape of the pulse height distribution, which only occurs if all the pixels triggered by an event in a cross-talk bunch produce identical bunches of Geiger pulses when after pulsing. Analogous to APD detector gain factors, there is additional noise associated with the gain factors for after pulsing and cross talk, σ_{a_n} and σ_x.

The after pulsing increases the fluctuations associated with the intensity of the events above that expected from shot noise [10]. We can approximate the magnitude of the fluctuation in the number of one-photon events using the after-pulsing gain factor, M_a and Equation 12, which assumes a simple correlation between the number of photons and the number of after pulses:

$$\sigma_a^2 \cong I\left(M_a + 2\sqrt{M_a - 1}\right). \tag{12}$$

The variable "I" represents the true photoelectron intensity. This approximation is valid when the after pulsing probability is less than 0.5 and is useful when we do not have a direct measurement of the after pulsing fluctuations, i.e., the second moment of the M_a distribution function.

The after pulsing affects the noise floor of the SSPM. Multiplying the I_d term in Equation 10 by M_a estimates the increase in the noise floor. Using the measured count rate, with out correcting for after pulsing, in Equation 10, provides a "first order" estimate of the effect of after pulsing on the noise floor in the SSPM.

The noise associated with the cross talk multiplier, σ_a, decreases the amplitude, or energy, resolution of the SSPM, and it increases the noise floor associated with the dark count signal. The probability distribution associated with cross talk is not a geometric distribution function because the sample size decreases as the size of the cross talk bunch increases. Nonetheless, the cross talk process may be similar enough to approximate the sigma associated with the cross talk by an analogy with after pulsing.

3. EXPERIMENTAL METHODS

In the quantum efficiency (QE) and profile-scan measurements, the CMOS GPD pixel is operated as a photodiode pixel. A focused HeNe laser, scanned across the pixel, measures the uniformity of the QE in the pixel.

The CMOS design integrates a 100-kΩ resistor with each of the pixel elements to quench the Geiger avalanche. This mode of operation is referred to as passive quenching and is used in all of the GPD measurements presented in this work. Measuring the onset of Geiger pulses when varying the bias voltage reveals the breakdown voltage of the GPD pixel.

The experimental details for measuring the radiometric performance and after pulsing in a single GPD pixel are described elsewhere [10], however, Figure 4 illustrates the experimental setup.
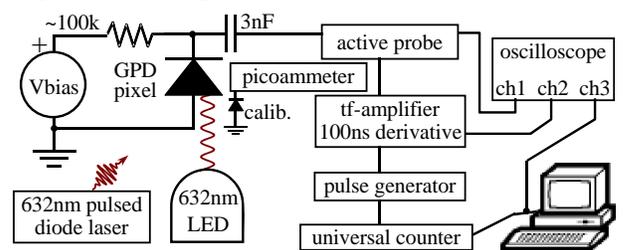
Figure 4: Illustration of the measurement setup. The photo-signal from the passively quenched 30-μm-diameter GPD pixel is amplified and differentiated by a timing-filter amplifier, denoted as "tf-amplifier" in the figure. The gain of the amplifier is adjusted to maintain constant amplitude for the average signal that triggers the pulse generator. A universal counter measures the Geiger pulse count rate.

The pair wise cross talk is measured as a function of excess bias and pixel spacing. For the operation as an SSPM, the arrays were designed with seven connected elements and two independent elements.

A pulsed 632-nm laser was used to measure the SSPM signal as a function of the illumination intensity. The output of seven pixels from two arrays are connected and fed into a multi-channel scaler (MCA) that is gated on the light pulse. The gating reduces the contribution of dark counts to the single photon event peak. This 14-pixel SSPM is operated at an excess bias of ~1 V.

4. RESULTS AND DISCUSSION

4.1. QE and Profile Scan

Figure 5 compares the quantum efficiency (QE) as a function of wavelength for two different pixel designs.
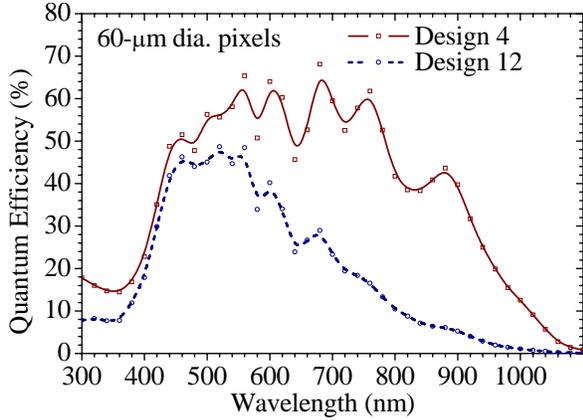
Figure 5: Plot for wavelength dependence of the quantum efficiency, where the CMOS APD pixel is operated as a unity gain photodiode, comparing the performance of two different pixel designs.

In the QE measurement, and profile scan described below, the pixels are operated as photodiodes. The plot shows that the design-4 pixel exhibits a better QE for red photons. This behavior is related to the depth of the pixel structure, where the design-4 pixel collects photoelectrons from the entire p-epitaxial layer, which is ~15 μm thick, where as the design-12 pixel only collects photoelectrons in the top 4 μm of the epitaxial layer. All of the subsequent data and analysis in this work uses the design-12 pixels.

Figure 6 shows a plot of the profile scan. In the figure, the dashed line, superimposed on the photograph of the 30-μm-diameter pixel, indicates that path of the laser spot. When the laser illuminates gaps in the top aluminum layer, the pixel detects light reflected between the metal and silicon surface, as indicated by the structure at -110 μm and the narrow peaks in the relative QE that flank the active area of the pixel.

A change in the reflectivity produces the slight QE variation in the active region of the pixel. The amount of light reflected back through the focusing optic is also plotted in Figure 6 and referenced to the axis on the right-hand side of the plot. The rough, top aluminum layer provides a reflective surface for coupling to scintillation materials.
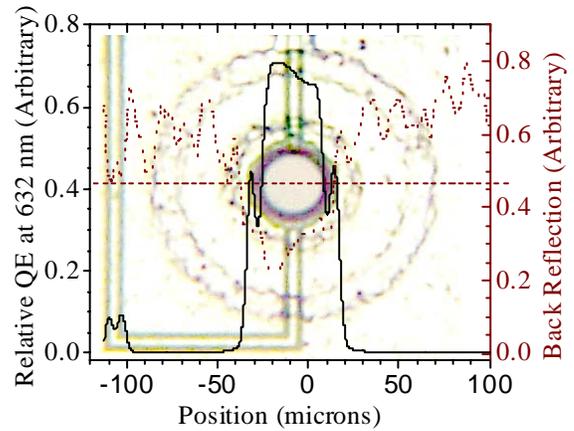
Figure 6: Profile scan of a focused 623-nam laser across the surface of a pixel. The dashed horizontal line illustrates the track of the laser across the pixel. The laser spot size is approximately 4-μm in diameter. The axis on the left plots the quantum efficiency, and the plot on the right plots the light reflected from the surface.

4.2. GPD Radiometeric Performance

The basic radiometric properties of the CMOS avalanche photodiodes have been measured for test pixels on each prototype chip. Typical results for a single 30-μm-diameter pixel show a detection efficiency of better than 20% at 632 nm, after correcting for after pulsing. The room temperature dark count rate for our best pixels is 0.5 kHz; the average is approximately 3 kHz.

Figure 7 shows the detection efficiency, at 632 nm, for the design-12 pixel, both before and after the application of the correction factor, as described by Equation 4.
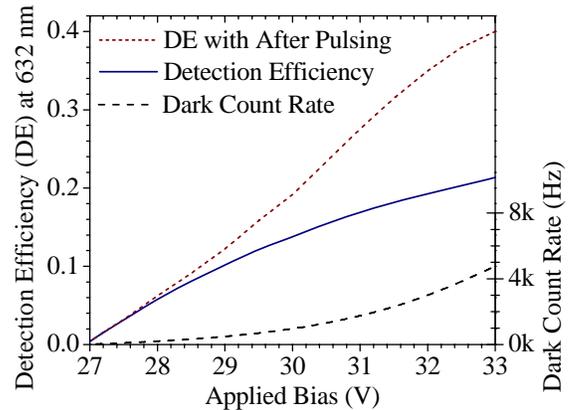
Figure 7: The single optical photon detection efficiency (DE) before, short red dash, and after, solid blue curve, correcting for the after pulsing. The measured "apparent DE" is corrected with the measured after pulse multiplier. Referenced to the axis on the right-hand side, the plot shows the dependence of the dark count rate (DCR), dashed black curve, on the applied bias.

As seen in the figure, the after pulsing increases the apparent DE with increasing applied bias. The figure also plots the dark count rate as a function of applied bias, which is referenced to the axis on the right-hand side of

the plot. The DE approaches the 632-nm QE of 25%, at an excess bias above 5V.

4.3. After-pulsing in a single pixel

After pulsing increases the measured count rate, and it also increases the fluctuations in the measured count rate. Figure 8 shows a plot of the measured fluctuations in the Geiger count rate, referenced to the axis on the left, together with the after pulse multiplication factor, M_a, referenced to the axis on the right.
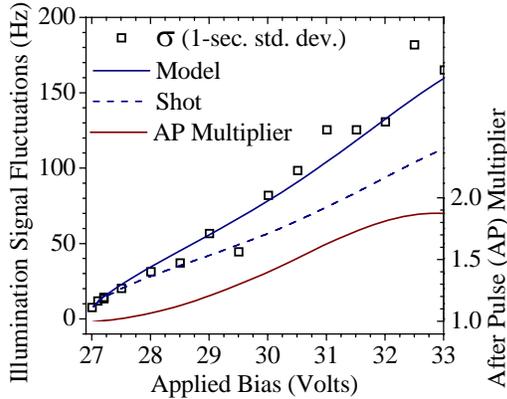
Figure 8: The fluctuations in the single photon count rate as a function of excess bias. In the graph, the dashed line shows the fluctuations expected for shot noise, and the solid line through the data is the model function, given by Equation 12. The lower curve plots the dependence of the after pulse multiplier, referenced on the right axis, on the applied bias.

As seen in the plot, the signal fluctuations, and the after pulse multiplication factor, M_a, increases with the applied bias. The plot also compares the magnitude of signal fluctuations expected from shot noise, as the square root of the measured rate (dashed line), to the fluctuation predicted by Equation 12 for correlated noise, the solid blue curve. Figure 8 shows that the expression for the fluctuations, in terms of the multiplication factor, provides a useful estimate because large statistical samples are required to experimentally recover precise values for the fluctuations; as indicated by the scatter in the experimental measurements.

4.4. Pair-wise Cross Talk

Measurements of the pair wise cross talk using dark counts and using external illumination produce similar results. Figure 9 shows the results of the illumination measurements and Equation 13 relates the percent pair wise cross talk, P_x, plotted in the figure, to the pair wise cross talk multiplication factor:

$$P_x = 1 - \frac{1}{m_x} = \frac{\alpha V_x}{r^2} . \tag{13}$$

The cross talk increases as a function of excess bias because the DE of the pixel increases, which increases the efficiency for detecting hot carrier emission from neighboring pixels. For the 150-µm-pixel spacing, the pair wise cross talk is less that 2% over the whole range of operating biases.
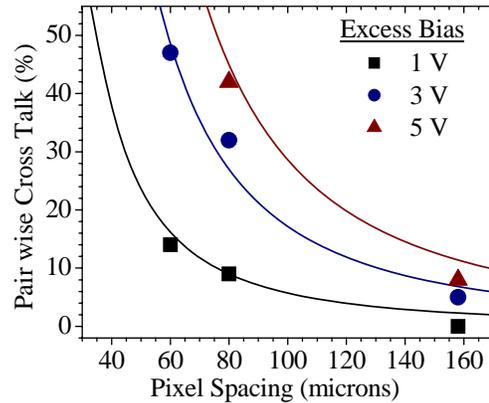
Figure 9: The cross talk between a pair of pixels, plotted as a function of the pixel pitch. The lines represent the fit of a simple function for P_x, using Equation 13, to the data points.

The lines through the data points represent the fit of the data to Equation 13, where the recovered value for α is 57,000 $\mu m^2/V$. This fit relates the anticipated cross talk gain to the design, specifically the pixel pitch and the operating conditions for the excess bias.

4.5. Light detection by SSPM detector

Varying the light incident on fourteen coupled pixels from a pulsed 632-nm laser produces a spectrum that shows one to fourteen pixels firing, depending on the intensity of the incident light. Figure 10 shows the pulse height distributions from the 14-element SSPM as the LED pulse amplitude is reduced with neutral density filters.
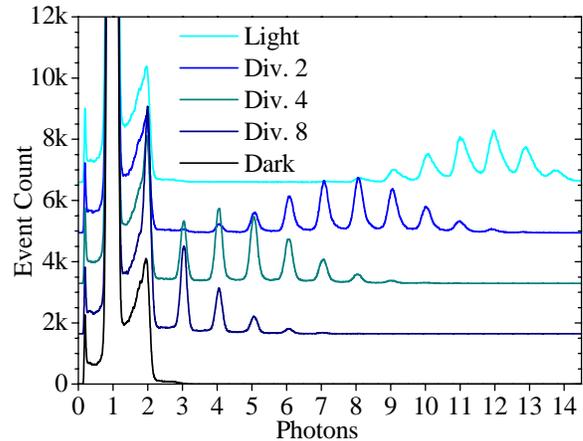
Figure 10: Light detection by a 14-pixel GPD array. The channel number corresponds to a pulse height from a multi-channel analyzer, gated by the input pulse to suppress dark counts. Each peak from left to right in the figure represents an additional pixel firing simultaneously. Fourteen peaks are visible in the data, the centroid of the distribution is seen to shift based on the light intensity.

In the plotted pulse height spectra, the mean position, or centroid of the distribution depends on the amplitude of the LED pulse. The clear resolution of the individual photon peaks in the distribution demonstrates the single-photon sensitivity of this small, 14-element SSPM. As the size and number of SSPM pixels increase, the noise floor associated with the increased dark count rate will obfuscate the signal from single optical photon events at room temperature.

4.6. SSPM Modeling

The initial modeling of the SSPM performance, as a function of design and operating conditions, addresses the following question: "What is the optimum pixel spacing for an SSPM detector with a fixed size of 2 mm×2 mm using 30-µm-diameter, design-12 CMOS GPD pixels?" Figure 11 plots the amplitude, or energy, resolution of the SSPM, which is referred to as the "number of effective pixels", as a function of pixel spacing for different excess bias settings.
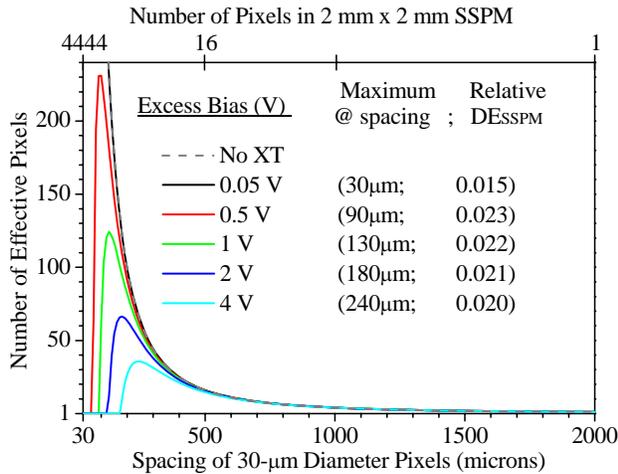
Figure 11: Model results for fixed area SSPM with varying pixel pitch. The cross talk measurements shown in Figure 9, above, were used to extrapolate the effect of pixel spacing on the SSPM energy resolution. The loss of resolution for close pixel spacing is a result of cross talk, and the loss for large pixel spacing is due to the area constraint.

Figure 11 also lists the relative DE for the SSPM at the different excess bias voltages for the listed pixel spacing, which correspond to the maxima in the plotted curves. The figure suggests that operating an SSPM with a pixel spacing of 90 µm at an excess bias of 0.5 V will yield an optimum performance. Although increasing the excess bias should increase the DE of the pixels, it also increases the amount of cross talk, which reduces the number of effective pixels, or energy resolution of the SSPM.

The cross talk between pixels in the SSPM, caused by hot carrier emission, represents a serious consideration in the design and operation of the SSPM devices because it can limit the fill factor, and thus the SSPM DE. Reducing the pixel size may reduce the hot carrier emission because the process is non-linear with current.

5. CONCLUSIONS

The CMOS-based SSPM provides a low-cost platform for integrated detector elements coupled to scintillation materials that can withstand harsh conditions, such as large magnetic fields. The SSPM detector can be applied to many imaging and detection applications, such as PET, SPECT, and direct gamma-camera applications, survey devices and rate-meters, digital dosimeter badges and portal scanning systems. The devices have a fast rise time, utilize inexpensive, high efficiency scintillation material with variable light output depending on the target application, and a low voltage operation that simplifies supporting electronics. Improving the SSPM DE, specifically the fill factor, and reducing the cross talk between pixels are key considerations in optimizing the design of SSPM devices.

Acknowledgments

References

[1] P. Buzhan, B. Dolgoshein, L. Filatov, A. Ilyin, V. Kantzerov, V. Kaplin, A. Karakash, F. Kayumov, S. Klemin, E. Popova, and S. Smirnov, "Silicon photomultiplier and its possible applications," *Nuclear Instruments and Methods in Physics Research, Section A*, vol. 504, pp. 48-52, 2003.

[2] S. Cova, M. Ghioni, A. Lacaita, C. Samori, and F. Zappa, "Avalanche photodiodes and quenching circuits for single-photon detection," *Appl.Opt.*, vol. 35, pp. 1956, 1996.

[3] S. Cova, A. Lacaita, and G. Ripamonti, "Trapping phenomena in avalanche photodiodes on nanosecond scale," *IEEE Electron Device Lett. (USA)*, vol. 12, pp. 685-7, 1991.

[4] S. Vasile, P. Gothoskar, R. Farrell, and D. Sdrulla, "Photon detection with high gain avalanche photodiode arrays," *IEEE Trans. Nucl. Sci. (USA)*, vol. 45, pp. 720-3, 1998.

[5] W. J. Kindt and H. W. Van Zeijl, "Modelling and fabrication of Geiger mode avalanche photodiodes," *IEEE Trans. Nucl. Sci. (USA)*, vol. 45, pp. 715-19, 1998.

[6] E. Sciacca, A. C. Giudice, D. Sanfilippo, F. Zappa, S. Lombardo, R. Consentino, C. Di Franco, M. Ghioni, G. Fallica, G. Bonanno, S. Cova, and E. Rimini, "Silicon Planar Technology for Single-Photon Optical Detectors," *IEEE Trans. Electron Devices*, vol. 50, pp. 918-25, 2003.

[7]   B. F. Aull, A. H. Loomis, D. J. Young, R. M. Heinrichs, B. J. Felton, P. J. Daniels, and D. J. Landers, "Geiger-mode avalanche photodiodes for three-dimensional imaging," *Linc. Lab. J. (USA)*, vol. 13, pp. 335-50, 2002.

[8]   J. C. Jackson, A. P. Morrison, D. Phelan, and A. Mathewson, "A novel silicon Geiger-mode avalanche photodiode," presented at International Electron Devices Meeting. Technical Digest (Cat. No.02CH37358), p. 797-800, 2002.

[9]   A. Rochas, M. Gani, B. Furrer, P. A. Besse, R. S. Popovic, G. Ribordy, and N. Gisin, "Single photon detector fabricated in a complementary metal-oxide-semiconductor high-voltage technology," *Rev. Sci. Instrum. (USA)*, vol. 74, pp. 3263-70, 2003.

[10]   C. J. Stapels, W. G. Lawrence, F. L. Augustine, and J. F. Christian, "Characterization of a CMOS Geiger Photodiode Pixel," *IEEE Transactions on Electron Devices*, vol. 53, pp. 631, 2006.

[11]   A. L. Lacaita, F. Zappa, S. Bigliardi, and M. Manfredi, "On the bremsstrahlung origin of hot-carrier-induced photons in silicon devices," *IEEE Trans. Electron Devices (USA)*, vol. 40, pp. 577-82, 1993.

[12]   L. Carbone, R. Brunetti, C. Jacoboni, A. Lacaita, and M. Fischetti, "Polarization analysis of hot-carrier light emission in silicon," *Semicond. Sci. Technol. (UK)*, vol. 9, pp. 674-6, 1994.

[13]   S. Villa, A. L. Lacaita, and A. Pacelli, "Photon emission from hot electrons in silicon," *Phys. Rev. B, Condens. Matter (USA)*, vol. 52, pp. 10993-9, 1995.